Strange metal from Gutzwiller correlations in infinite dimensions

Wenxin Ding, Rok Žitko, Peizhi Mai, Edward Perepelitsky, and B. Sriram Shastry

Phys. Rev. B **96**, 054114 — Published 18 August 2017

DOI: 10.1103/PhysRevB.96.054114

A Strange Metal from Gutzwiller correlations in infinite dimensions

Wenxin Ding[1], Rok Žitko [2,3], Peizhi Mai[1], Edward Perepelitsky[1] and B Sriram Shastry[1]
[1] *Physics Department, University of California, Santa Cruz, California, 95060,*
[2] *Jožef Stefan Institute, Jamova 39, SI-1000 Ljubljana, Slovenia*
[3] *Faculty for Mathematics and Physics, University of Ljubljana, Jadranska 19, SI-1000 Ljubljana, Slovenia*
(Dated: June 12, 2017)

Recent progress in *extremely correlated Fermi liquid theory (ECFL)* and the *dynamical mean field theory (DMFT)* enables us to accurately compute in the $d \to \infty$ limit the resistivity of the t-J model after setting $J \to 0$. This is also the $U = \infty$ Hubbard model. Since J is set to zero, our study isolates the *dynamical effects* of the single occupation constraint enforced by the projection operator originally introduced by Gutzwiller. We study three densities $n = .75, .8, .85$ that correspond to a range between the overdoped and optimally doped Mott insulating state. We delineate four distinct regimes separated by three crossovers, which are characterized by different behaviors of the resistivity ρ. We find at the lowest temperature T a *Gutzwiller Correlated Fermi Liquid* regime with $\rho \propto T^2$ extending up to an effective Fermi temperature that is dramatically suppressed from the non-interacting value by the proximity to half filling, $n \sim 1$. This is followed by a *Gutzwiller Correlated Strange Metal* regime with $\rho \propto (T - T_0)$, i.e. a linear resistivity extrapolating back to $\rho = 0$ at a positive T_0. At a higher temperature scale this crosses over into the *Bad Metal* regime with $\rho \propto (T + T_1)$, i.e. a linear resistivity extrapolating back to a finite resistivity at $T = 0$, and passing through the Ioffe-Regel-Mott value where the mean free path is a few lattice constants. This regime finally gives way to the *High T Metal* regime, where we find $\rho \propto T$, i.e. a linear resistivity extrapolating back to zero at $T = 0$. The present work emphasizes the first two, i.e. the two lowest temperature regimes, where the availability of an analytical ECFL theory is of help in identifying the changes in related variables entering the resistivity formula that accompany the onset of linear resistivity, and the numerically exact DMFT helps to validate the results. We also examine thermodynamical variables such as the magnetic susceptibility, compressibility, heat capacity and entropy, and correlate changes in these with the change in resistivity. This exercise casts valuable light on the nature of charge and spin correlations in the Gutzwiller correlated strange metal regime, which has features in common with the physically relevant strange metal phase seen in strongly correlated matter.

I. INTRODUCTION

The resistivity due to mutual collisions of electrons at low temperatures reveals the lowest energy scale physics of charge excitations in metallic systems, and therefore is very important. While it is fairly straightforward to measure experimentally, it is also one of the most difficult quantities to calculate theoretically, especially if electron-electron interactions are strong. Motivated by the unexpected behavior of resistivity and other variables in cuprate superconductors and related two-dimensional experimental systems, some works have postulated that the Fermi liquid theory - originally developed and justified for weakly interacting systems - would break down. In its place a zoo of non-Fermi liquids have been postulated, without necessarily having a rigorous theoretical underpinning. On the other hand the analytical framework of the extremely correlated Fermi liquid theory (ECFL)[1] and the well established dynamical mean field theory (DMFT)[2] give a different type of result, where the strong interactions compress the regime of Fermi-liquid type variation to a very small temperature and frequency scale. This Fermi-liquid regime is succeeded by a variety of regimes that display unusual non-Fermi-liquid dependences on frequency and temperature. The main goal of this work is to elucidate and characterize the different regimes that arise in the ECFL and DMFT theories, and to provide a quantitative comparison between the qualitatively similar results of these two theories, as applied to the infinite-dimensional Hubbard model, with the Hubbard charge repulsion parameter U taken to infinity, $U \to \infty$.

In earlier work[3] we have compared the ECFL and DMFT results for the zero-temperature spectral functions, finding an encouraging similarity. On scaling the frequency with the respective quasiparticle weights Z of the two theories the agreement is even close to quantitative. In the present work we undertake the more ambitious comparison of the resistivity and thermodynamic variables at finite temperatures.

In both the ECFL theory and the DMFT, the strong interactions cause the quasiparticles of the lowest temperature Fermi liquid to become fragile, i.e., the resulting quasiparticle weight Z is very small, $Z \ll 1$. This is also arguably the relevant regime in contemporary materials such as cuprate superconductors, and hence interest in this problem is very high.

In the problem studied here, namely $U \to \infty$ and $d \to \infty$, the DMFT theory is formally exact. Further, the possibility of computing the resistivity from the sole knowledge of the single-particle Green's function is enabled by the vanishing of vertex corrections[4]. Despite these simplifications, obtaining *reliable* results for the resistivity is technically formidable due to the requirement

of an impurity solver providing accurate and reliable results for the self-energy function Σ on the real frequency axis for both very low and very high temperatures. This problem has only recently been solved in Ref. (5), almost 25 years after the formulation of the DMFT theory. The resistivity of the Hubbard model is now known for all densities and all values of U, including $U = \infty$. This is the first set of exact results for the resistivity in interacting metallic systems resulting from inelastic scattering, and therefore represent an important advance in the field. The DMFT results[5,6] offer a unique opportunity to test a variety of techniques and approximate methods for computing this variable. The ECFL formalism, on the other hand, is in its early stages of development and several technical innovations are ongoing so as to enable reliable calculations in the challenging regimes of the density $n \lesssim 1$[3,7].

Lastly, in a recent work Ref. (8) our group has published a voluminous high-temperature study using series expansion techniques adapted for very strong correlations, thus extending our understanding of the resistivity to the full range of temperatures. This study is on the same model as the present work and extends the results of Ref. (5) to much higher temperatures. In these studies the effect the superexchange J is absent due to the $U = \infty$ limit, and therefore there is no superconducting regime that one might expect from a t-J model in finite dimensions. By taking the limit of infinite U we have also banished the static superexchange that the DMFT includes for finite U[9–17]. However, these studies *do* capture the notoriously difficult non-perturbative local Gutzwiller correlation effects on the resistivity quantitatively, for the first time. It seems fair to say that our understanding of the strong correlation problem has advanced significantly with these recent works.

In summary, at the lowest temperatures these earlier studies[5–8] found a Fermi-liquid type resistivity with $\rho \propto T^2$. This regime extends only up to $T_{FL}(\delta)$, a Fermi-liquid temperature scale dependent on the hole density ($\delta \equiv 1 - n$). We shall term this the *Gutzwiller Correlated Fermi Liquid* (GCFL) regime. This regime is followed by three distinguishable regimes with linear in T resistivity having different slopes and intercepts, which are separated by crossovers; a *Gutzwiller Correlated Strange Metal* (GCSM) followed by a "Bad Metal" and finally a "High-T metal" regime, as discussed below (see Fig. (1)). The nomenclature stresses that these regimes originate purely from Gutzwiller correlations (i.e., double occupancy avoidance). In particular the regimes have no dependence upon the superexchange energy J or other energy scales which might be additionally involved in producing the related strange metal found in cuprates[18,19].

In order to understand the low-temperature regimes, we would like to throw light on the factors that lead to an extraordinarily low values of the Fermi temperature $T_{FL}(\delta)$ that are found. We also wish to provide a detailed understanding of the behavior of constituent variables that lead to a linear resistivity in the GCSM regime, starting at this low temperature. Here the ECFL theory provides us with a great advantage since it is largely analytical, and one can inspect the various constituents in detail. It is also interesting to seek a possible causal relationship between the linear temperature dependence of ρ in the GCSM regime and the nature of incipient order (either spin or charge) that might be present. For this purpose, it is useful to compute, by using the techniques of Ref. (5 and 7), the entropy and heat capacity, the magnetic susceptibilities and compressibility. For completeness we also study the thermoelectric transport, as well as a few dynamical quantities such as the self energy of the electrons. In a following paper we present other dyamical variablse such as the optical conductivity. These quantities provide a complete picture of the metallic states having various temperature dependences sketched in Fig. (1).

The lowest temperature *Gutzwiller-correlated Fermi*

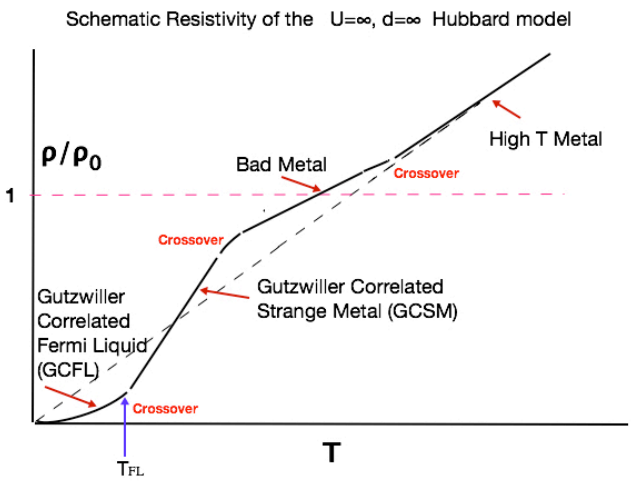

FIG. 1. A schematic view of the different regimes of temperature dependent resistivities found in the calculations of Ref. (5–8). The various temperature scales are schematic. At the lowest T we have a Gutzwiller-Correlated-Fermi liquid regime (GCFL) with $\rho \propto T^2$. This quadratic variation terminates at a characteristic Fermi temperature $T_{FL}(\delta)$, which is found to be surprisingly small relative to $T_{BR} = \delta D$, the Brinkman-Rice temperature scale ($2D$ is the bandwidth). Upon warming we reach the Gutzwiller-Correlated-Strange metal (GCSM) regime, which is the main focus of this work. This gives way at higher T to the so called bad-metal regime with a resistivity that increases linearly beyond the Ioffe-Regel-Mott value ρ_0 characteristic of disordered metals. The temperature scale of this regime is T_{BR} discussed above. Finally at the highest T we reach the high T regime with $\rho \propto T$ that can be extrapolated back to pass through the origin. We thus find a total of four regimes separated by three crossovers. It should be noted that in both theories considered here, the approximate range of the temperatures scales are $T_{FL} \sim 0.004 - 0.01D$, and the crossover to the bad-metal regime occurs at $T \sim 0.04 - 0.06D$ for the densities considered ($n = 0.75$ to $n = 0.85$).

liquid (GCFL) with $\rho \propto T^2$ shows enhancements of certain static susceptibilities that are similar to those of the normal state of liquid ^{3}He. The *almost localized Fermi liquid theory* (ALFL) of these enhancements is discussed by Vollhardt, Wölfle and Anderson in Ref. (24 and 25) on the basis of Gutzwiller's wave function and its approximation to the Hubbard model, where the variation of the Landau parameters with density at fixed (large) U is considered. In particular Ref. (25) studies the enhancements of Fermi liquid parameters leading to enhanced effective mass m^*/m, magnetic susceptibility $\chi_{spin}/\chi^0_{spin}$ and the bulk modulus (i.e. the inverse compressibility). Within the ALFL all the three stated enhancements *are* proportional to the inverse of Z in that theory as well as in ^{3}He. We check below the extent to which this is true in the GCFL regime, to see how it compares with the predictions of the ALFL theory, and find that the behavior of the compressibility is somewhat different.

Upon warming we reach the GCSM regime with a linear temperature dependence of the resistivity ρ. This regime is interesting since it is reminiscent of the *strange metal* regime in the cuprate phase diagrams[18]. It is remarkable that this linear resistivity regime extends to very low T, essentially the $T_{FL}(\delta)$, and one wants to know if this behavior is causally linked to a change in entropy, i.e. to disordering. We aim at correlating the GCSM regime with the extent of short ranged spin or charge order in this regime. These should be reflected in the heat capacity and the entropy gain. By computing these variables, we show that upon warming from $T = 0$ substantial entropy is released as we reach T_{FL}. However in the entire GCSM regime the magnetic susceptibility is Pauli like, i.e., with an approximately T independent behavior, and hence spin entropy should be unchanged. From a high-T expansion and on various general grounds, it is known that it changes into a Curie-Weiss type behavior at the onset of the bad-metal regime.

The GCSM regime is followed by other subtly different T dependences as described in Sec. III A that obtain in the bad-metal regime and the high-temperature regime. The density dependences of the various crossover scales give important insight into the physics of the resistivity. With one exception, all calculations reported here are performed using both ECFL and single-site DMFT methods. Using the two methods is very important since it gives us the opportunity to benchmark the mostly analytical and relatively new ECFL technique with the established and largely numerical DMFT method. The magnetic susceptibility is available only from DMFT, and our presentation below seems to be the most extensive result for this subtle variable reported to date[11,26,27].

The plan of the paper is as follows. In Sec. II we first make some further technical remarks about the methods. In Section III A we describe the various T dependences of the resistivity which serve to define the GCFL and GCSM regimes, and also point to the higher T bad-metal and high-T regimes. In Section III B we compare the chemical potential and compressibility. In Section III C we discuss the frequently made bubble approximation for the charge and spin susceptibilities, and show that the bubble susceptibility is exactly expressible as an integral of the energy derivative of momentum distribution function in $d = \infty$. We also note that it is a good approximation to the exact result for the charge susceptibility, but not so for the spin susceptibilty. In Section III D we illustrate the self energy and local density of states from the two methods, and find that within ECFL the quasiparticles tend to have somewhat smaller Z at the highest densities, as compared to DMFT. This causes a few other differences described later. In Section III E we examine further T dependent properties, the heat capacity and entropy. Section III F discusses the magnetic susceptibility χ from the DMFT calculations and lists some of the technical difficulties that prevent its evaluation in the ECFL theory. In Section III G we discuss the thermoelectric transport coefficients, the Seebeck coefficient and the Lorenz number as well as the thermoelectric efficiency. In Section IV we discuss the salient features of our results.

II. METHODS

In ECFL we have thus far used an expansion in the parameter λ, which plays a role analogous to the quantum parameter $\frac{1}{2S}$ in quantum theories of magnetism, where S is magnitude of the spin. In the first DMFT-ECFL comparison paper Ref. (3), we used the second order terms in an expansion in λ. This approximation led to quantitatively reliable answer for the quasiparticle weight Z at low temperature only in the overdoped regime $n \lesssim .75$, but to a non-vanishing value of Z for $n \to 1$. In the more recent paper Ref. (7) this problem was addressed using the exact, rather than the λ^2 version of the hole number sum rule, together with a cut-off for the tails of the spectral function at very high energies. This procedure extends the validity of the second order terms to higher density $n \lesssim 0.85$, so that the Z values at low T tend to zero as the insulating state is approached and are comparable to, if somewhat smaller than, the DMFT results. Due to this improvement, we found that the resistivity is now on the same scale, and exhibits very similar crossover features as the results in Ref. (5 and 6), as detailed below. In this work we report the comparison between the T dependent resistivity and other thermodynamic variables found from this cutoff scheme[28] and the exact results from DMFT. We use the Bethe lattice semi-circular density of states $D(\epsilon) = \frac{2}{\pi D}\sqrt{1-\epsilon^2/D^2}$ in both theories.

The ECFL scheme used here has been described in detail in Ref. (7), and consists of using the $\mathcal{O}(\lambda^2)$ expansion with the full number sum rule and the Tukey window used to cut off the spectral width at very high energies.

The DMFT scheme has been described in detail in Ref. (3). The NRG calculations[29,30] in this work were performed with the discretization parameter $\Lambda = 2$, us-

ing the discretization scheme from Refs. 31 and 32 with $N_z = 16$ interleaved discretization grids. The truncation cut-off was set at $10\omega_N$, where ω_N is the characteristic energy scale at the N-th step of the iteration. We used charge conservation and spin SU(2) symmetries. The spectral functions were computed with the full-density-matrix algorithm[33] and broadened with a log-Gaussian kernel with $\alpha = 0.05$, followed by a Gaussian kernel with $\sigma = 0.3T$. The occupancy was controlled using the Broyden method[34]. The self-energy was computed through the ratio of correlators, $\langle\langle n_{\bar\sigma} d_\sigma; d^\dagger_\sigma\rangle\rangle / \langle\langle d_\sigma; d^\dagger_\sigma\rangle\rangle$[35], corrected by the term $-w_{\rm UHB}/\langle\langle d_\sigma; d^\dagger_\sigma\rangle\rangle$, where $w_{\rm UHB}$ is the spectral weight of the upper Hubbard peak which was outside the NRG energy window (we redid some calculations using the standard approach that explicitly includes the UHB in the every window, using a very large but finite value of U; we found excellent agreement between the two computational schemes).

III. RESULTS

In this work we consider the temperature region $T \leq 0.02D$, which covers the range up to 200 K if we assume $D \sim 10000$ K, i.e. $\mathcal{O}(1)$ eV. Here D is the half bandwidth. We study three densities (number of electrons per site) $n = 0.75, 0.8, 0.85$. These are typical of the over-doped and optimally doped cuprates.

A. DC Resistivity

We begin with a summary of the results for the resistivity which form the bedrock for this study. The findings in Ref. (5–7) are extended in Ref. (8) to higher temperatures, and from these we have a fairly complete understanding of the behavior of ρ at *essentially all* T. A cartoon of these is sketched in Fig. (1). The resistivity exhibits a variety of dependences on T upon warming from the absolute zero: (i) the Gutzwiller correlated Fermi liquid (GCFL) regime with a quadratic T dependence $\rho \propto T^2$ up to a (hole) density-dependent Fermi-liquid temperature $T_{FL}(\delta)$ ($\delta = 1 - n$); (ii) the Gutzwiller-correlated-strange metal (GCSM) regime with a linear T dependence $\rho \propto T +$ constant (constant < 0), (iii) a "knee" connecting to the bad-metal (BM) regime with again a linear T dependence $\rho \propto T +$ constant (constant > 0). This regime is so named since the ρ crosses the fiduciary Ioffe-Regel-Mott maximal resistance ρ_0 at temperature on the order of the Brinkman-Rice energy δD, followed by (iv) a crossover to a high-temperature regime again with linear T dependence $\rho = AT$, devoid of an offset so that the line extrapolates back to pass through the origin.

In Fig. (2) we present the resistivity in the GCFL and GCSM regimes. It is striking that the GC strange metal has a robust linear T resistivity over a wide T scale. The linear resistivity begins at $T_{FL}(\delta)$ which can be driven

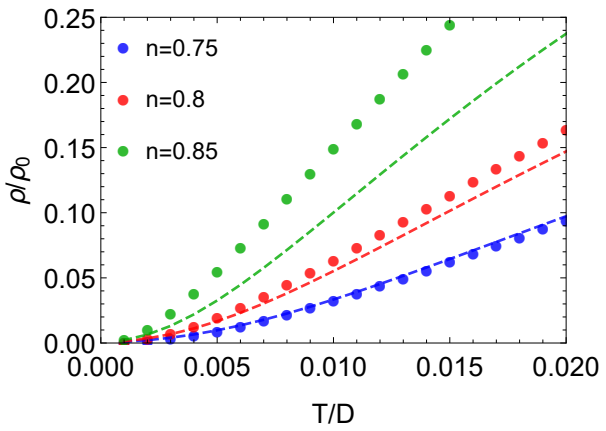

FIG. 2. Comparison of the resistivity computed using the ECFL (symbols) and the DMFT (dashed). $\sigma_0 = 1/\rho_{IRM}$ is the Ioffe-Regel-Mott conductivity. As n gets closer to unity, the ECFL scheme employed systematically underestimates Z relative to the exact DMFT values (see Fig. (6) Ref. (7)). This lowers the effective Fermi temperature T_{FL}, and simultaneously enhances the magnitude of ρ for $T > T_{FL}$ a feature that is prominently visible above. It should be possible to improve the quantitative agreement between the two theories in future[28].

to low values, $\sim$ 45K (see Ref. (7)), by the Gutzwiller correlations alone, even though the bandwidth is of $\mathcal{O}(2)$ eV. We emphasize that this unexpectedly drastic scale reduction yielding $T_{FL} \ll ZD \ll \delta D$ requires a "hard" calculation for justification, and can hardly be argued from general principles. The slight difference in the $T_{FL}(\delta)$ between the two theories is due to the somewhat different $Z(\delta)$ found in the two theories, for example Fig. (6) of Ref. (7) shows that the ECFL gives a smaller Z than the DMFT[28]. We also note that using the standard value for $\rho_{IRM} \sim 300$ $\mu\Omega$ cm, the Ioffe-Regel-Mott resistivity Ref. (36), the absolute scale of the resistivity computed in these approaches is quite similar to that found in the experiments. For example, Fig. (1) in Ref. (7) compares well on an absolute scale with the well-known linear resistivity result of S. Martin *et. al.* in Ref. (37) on Bi2212, where the superconducting phase cuts off the region $T \leq 80$K.

Building on the analysis of Refs. (5–7), we derive a closed form expression for the resistivity in terms of the chemical potential and the real and imaginary parts of the single-particle self-energy on the Fermi surface (Eq. (7)). We begin with the formula (Eq. (41) in Ref. (7)) for the conductivity on the infinite-dimensional Bethe lattice:

$$\sigma = 2\pi D\ \sigma_0 \int d\omega \int d\epsilon \left(-\frac{\partial f}{\partial \omega}\right) \phi(\epsilon) \rho_G^2(\epsilon, \omega), \qquad (1)$$

where $\sigma_0 = e^2\hbar\Phi(0)/D$ (Φ is defined in Eq. (39) of Ref. (7)), $\sigma_0 \sim 1/\rho_{IRM}$, and the transport function $\phi(\epsilon) = \Phi(\epsilon)/\Phi(0)$ is given explicitly in Eq. (40) of Ref. (7) as $\phi(\epsilon) = \Theta(1 - \frac{\epsilon^2}{D^2}) \times (1 - \frac{\epsilon^2}{D^2})^{\frac{3}{2}}$. The single-particle

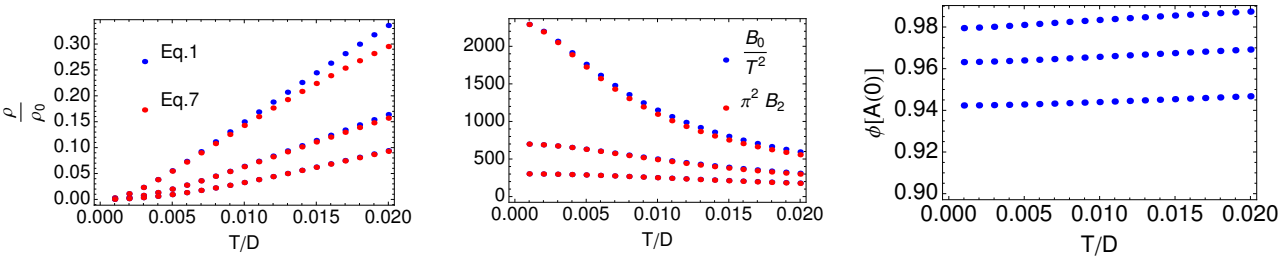

FIG. 3. ECFL calculation of the resistivity and related objects. **Panel a)**: The resistivity as a function of the temperature using the exact formula, Eq. (1), compared with the approximation, Eq. (7), for $n = 0.75,\ 0.8,\ 0.85$ (bottom to top). Eq. (7) is an excellent approximation at all densities for all temperatures. **Panel b)**: Parameters resulting from a low-frequency expansion of the imaginary part of the self-energy in the vicinity of the Fermi-surace, plotted as a function of temperature, for $n = 0.75,\ 0.8,\ 0.85$ (bottom to top). B_0 is the self-energy on the Fermi surface, while B_2 is the quadratic-frequency term. The ratio $\frac{B_2\pi^2T^2}{B_0} \to 1$ as $T \to 0$, and is approximately constant as a function of temperature. **Panel c)**: $\phi[A(0)] = \phi[\mu - \Re e\Sigma(0)]$, plotted as a function of the temperature, for $n = 0.75,\ 0.8,\ 0.85$ (bottom to top). $\phi[A(0)]$ is practically independent of temperature, and has very weak density-dependence.

spectral-function is

$$\rho_G(\epsilon,\omega) = \frac{1}{\pi}\frac{B(\omega)}{\left[A(\omega)-\epsilon\right]^2 + B^2(\omega)}, \tag{2}$$

where $A(\omega) \equiv \omega + \mu - \Re e\,\Sigma(\omega)$, $B(\omega) = -\Im m\,\Sigma(\omega)$, and all objects depend implicitly on the temperature T. At low temperatures and frequencies $B(\omega) \ll D$, so that Eq. (1) simplifies to

$$\sigma = \sigma_0 \int d\omega \left(-\frac{\partial f}{\partial \omega}\right) \frac{\phi\left[A(\omega)\right]}{B(\omega)}, \tag{3}$$

Following[6], we perform a small-frequency expansion

$$\phi\left[A(\omega)\right] = \phi\left[A(0)\right] + \ldots; \qquad B(\omega) = B_0 + B_2\,\omega^2 + \ldots. \tag{4}$$

The linear order term in $B(\omega)$ as well as all higher order terms in $B(\omega)$ and $\phi\left[A(\omega)\right]$ make negligible contributions to the conductivity in the temperature range considered, and are therefore neglected. The integral may be evaluated analytically and yields

$$\sigma = \frac{\sigma_0\ \phi\left[A(0)\right]}{2\pi T\sqrt{B_2 B_0}}\ \psi_1\left(\frac{1}{2} + \frac{1}{2\pi T}\sqrt{\frac{B_0}{B_2}}\right), \tag{5}$$

where $\psi_1(z)$ is the Polygamma function, related to the Digamma function, $\Psi(z)$, through $\psi_1(z) \equiv \frac{d}{dz}\Psi(z)$[38]. The ratio $\frac{B_0}{B_2\pi^2T^2}$ is weakly-dependent on temperature, and may be replaced by its zero-temperature limit (Fig. (3b)). In order to find this limiting value, consider the GCFL regime where

$$B_0 = B_2\pi^2T^2 \quad (GCFL). \tag{6}$$

Substituting Eq. (6) into Eq. (5) and eliminating B_2, we finally obtain the simple formula

$$\rho = \frac{12\ \rho_0}{\pi^2\ \phi\left[\bar{\mu} - \Re e\ \bar{\Sigma}(0)\right]} \times B_0, \tag{7}$$

where we have used that $\psi_1(1) = \frac{\pi^2}{6}$. Here, we denote the zero-temperature limit of any variable Q as $\bar{Q}$, and have used that $\phi\left[A(0)\right]$ is practically temperature-independent (Fig. (3c)). Hence, the resistivity is proportional to the imaginary part of the self-energy on the Fermi-surface. Moreover, the proportionality constant is very weakly density-dependent (since this is true of $\phi\left[\bar{A}(0)\right]$). Eq. (7) can be obtained from Eq. (47) in Ref. (7) by multiplying the RHS of the latter by the constant $\frac{12}{\pi^2}$ and setting $T \to 0$ in the denominator. The latter equation is obtained by retaining the leading order term in the Sommerfeld expansion of Eq. (3). In Fig. (3a), we plot the resistivity as a function of the temperature, using both Eqs. (1) and (7), in the ECFL scheme. We find that Eq. (7) is an excellent approximation at all densities and temperatures considered, i.e. it holds in both the GCFL and GCSM regimes.

In the GCFL regime, substituting Eq. (6) into Eq. (7), and using the fact that B_2 is approximately constant, we find that

$$\rho = \frac{12\bar{B}_2\ \rho_0}{\phi\left[\bar{A}(0)\right]} \times T^2 \quad (GCFL). \tag{8}$$

From Fig. 7 of Ref. (7), we know that $\bar{B}_2 \propto \frac{1}{\bar{Z}^2}$, where Z is the quasiparticle weight on the Fermi-surface. Therefore, Eq. (8) implies that $\rho \propto \frac{T^2}{\bar{Z}^2}$ in the GCFL regime.

In Fig. (4), we plot the exact resistivity, together with the approximation Eq. (7), both obtained using the DMFT calculation (corresponding to Fig. (3a) in the case of ECFL). Once again, we find that Eq. (7) is an excellent approximation at all densities and temperatures considered, i.e. it holds in both the GCFL and GCSM regimes.

Finally, we note that the important effective Fermi temperature, T_{FL}, can be estimated as the temperature at which the resistivity deviates from its low-temperature quadratic behavior. We find at the three densities con-

sidered, the so determined effective Fermi temperature for ECFL is, in agreement with Ref. (7), given by $T_{FL} \sim .05\bar{Z}D$. In the case of DMFT, we also find $T_{FL} \sim .05\bar{Z}D$, where a slightly higher value of $\bar{Z}$ results in a slightly higher value of T_{FL}, as compared to ECFL.

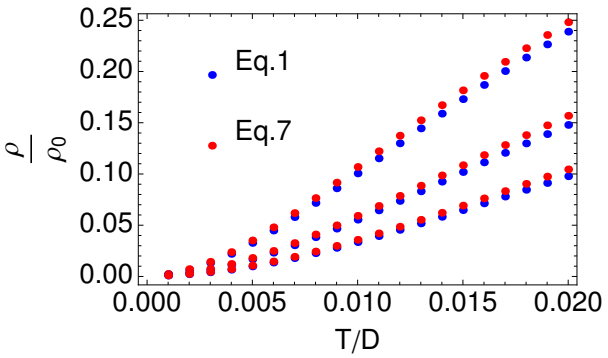

FIG. 4. The exact resistivity (Eq. (1)) compared with the approximation Eq. (7), using the DMFT calculation for $n = 0.75,\ 0.8,\ 0.85$ (bottom to top). Eq. (7) is an excellent approximation at all densities for all temperatures. (See Fig. (3a) for the corresponding figure in ECFL.)

B. Chemical potential and compressibility

The chemical potential in the ECFL theory is found from the self-consistency condition of the Green's function. The compressibility $\kappa = n^{-2}\partial n/\partial\mu$ is determined by numerical differentiation. The derivative is computed using the finite difference formula $\partial n/\partial\mu = [(n+\delta n) - n]/[\mu(n+\delta n) - \mu(n)]$ with $\delta n = 0.001$. In the DMFT we used larger $\delta n = 0.01$ and we performed two full DMFT runs for fillings n and $n + \delta n$.

We see that the chemical potentials (Fig. 5) match well apart from a constant shift[39]. The results obtained using two different impurity solvers (NRG and CT-HYB QMC) in the DMFT are in agreement, thus the difference is not related to some technical issue in the NRG, but is an actual discrepancy between DMFT and ECFL.

In our earlier work on the single impurity Anderson model[40], using a scheme that is an adaptation of that in Ref. (3), we studied the single impurity energy, which is a close analog of the chemical potential in the present problem. There we found that the location of the impurity energy found from the 2nd order ECFL equations matched very closely the impurity energy found in the NRG (see Table-1 Ref. (40)). In view of that excellent agreement, the current discrepancy on the absolute scale of the chemical potential between the DMFT results (also from NRG) and the present second order scheme is somewhat unexpected. It would appear that the different hole number sum rule and the cutoff scheme used here relative to the scheme in Ref. (3 and 40) influences this variable- and needs to be investigated more closely in future.

We note that the compressibilities (Fig. 6) are also roughly similar, and both theories show a suppression relative to the free fermion theory. The free fermion theory shows a slight monotonic decrease of the compressibility with T. In the GCFL and GCSM regimes, the ECFL compressibility shows an increase with T, followed by a slight fall with T in the bad metal regime. In (6b), we show that in the ECFL theory Z/κ is a constant within numerical errors ($\sim \pm 3.4\%$) at $T = 0.001D$. This is not the case in the DMFT, where Z is proportional to δ, while κ behaves approximately as $\kappa \propto \delta^{0.2}$ close to the doping-driver Mott transition[3]. In the GCFL regime, if we assume that the limit $n \to 1$ follows the almost localized Fermi liquid theory[24,25], we should expect the compressibility to scale with Z. This is in accord with the results of ECFL Fig. (6) panel (b), but not with the DMFT.

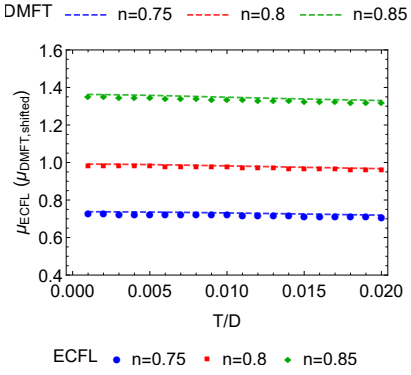

FIG. 5. Chemical potentials at $n = 0.75,\ 0.8,\ 0.85$ for ECFL (symbols) and DMFT (dashed lines). The DMFT results are shifted by a density-dependent constant. After the shift, the chemical potentials almost coincide.

C. Bubble Susceptibility

The knowledge of the Green's functions and the numerically determined exact compressibility and magnetic susceptibility χ_{spin} (see below Section(III F)) enable us to check a popular assumption of retaining only the bubble graphs, and throwing away the vertex correction for these quantities. We write the charge susceptibility $\chi_c = dn/d\mu$ as

$$\chi_c = \frac{1}{\beta N_s}\frac{d}{d\mu}\sum_{k,\omega_n,\sigma} e^{i\omega_n 0^+} G_\sigma(k, i\omega_n)$$
$$= -\frac{1}{\beta N_s}\sum_{k,\omega_n,\sigma} G^2_\sigma(k, i\omega_n)\{1 - \frac{d}{d\mu}\Sigma_\sigma(k, i\omega_n)\} \quad (9)$$

and similarly for χ_{spin} by replacing $\frac{d}{d\mu} \to \frac{d}{dB}$, where B is the magnetic field. The vertex corrections thus correspond to the μ or B derivatives of the *self energy*. Approximating this by dropping the derivative of the self

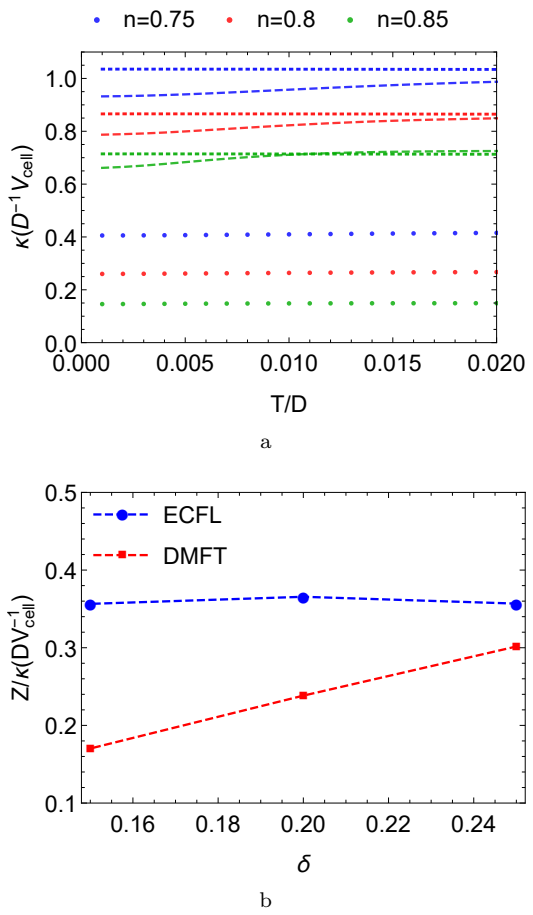

FIG. 6. (a) Compressibility $\kappa = n^{-2}\partial n/\partial\mu$ of ECFL (symbols), DMFT (dashed lines) and free fermions (dotted lines). The DMFT results give a systematically higher value of compressibility than the ECFL theory. (b) Z/κ for the lowest temperature $T = 0.001D$ at the three densities considered for ECFL (blue) and DMFT (red). The ECFL result for the compressibility is proportional to the quasiparticle weight Z, unlike the DMFT result which displays some variation. The difference in compressibility between the two theories seems related to the density dependent shift in chemical potentials noted in Fig. (5).

energy, we get $\chi_c \sim \chi_{spin} \sim \chi_{Bubble}$ where

$$\chi_{Bubble} = -\frac{1}{\beta N_s}\sum_{k,\omega_n,\sigma} G^2_\sigma(k, i\omega_n). \tag{10}$$

As usual we can convert the sum to a contour integral using the pole structure of the Fermi function $f(\omega)$ and write

$$\chi_{Bubble} = \frac{2}{N_s}\sum_k \int_\Gamma \frac{d\omega}{2\pi i} f(\omega) G^2(k,\omega) = \frac{2}{\pi N_s}\sum_k \int d\omega f(\omega)\Im m\, G^2(k,\omega+i0^+), \tag{11}$$

where Γ is a closed contour encircling the imaginary axis in a counterclockwise fashion, and we rotated the axis to a pair of lines parallel to the real axis to obtain the final line. Using the standard definition of the spectral function $\rho_G(k,\omega) = -\frac{1}{\pi}\Im m\, G(k,\omega+i0^+)$ we may write $\Im m\, G^2(k,\omega+i0^+) = (-2\pi)\Re e\, G(k,\omega)\ \rho_G(k,\omega)$ to express $\chi_{Bubble} = -\frac{4}{N_s}\sum_k \int d\omega f(\omega)\Re e\, G(k,\omega)\rho_G(k,\omega)$. In the limit $d\to\infty$ the Dyson self energy is independent of k, and therefore we can write $\Im m\, G^2(\epsilon,\omega+i0^+) = \Im m\, \frac{d}{d\epsilon}G(\epsilon,\omega+i0^+) = -\pi\frac{d}{d\epsilon}\rho_G(\epsilon,\omega)$, where we exchanged the two operations in the last line. Using the definition of the single particle momentum distribution function $n_k \to n(\epsilon) \equiv \int d\omega f(\omega)\rho_G(\epsilon,\omega)$ we can perform the ω integration in Eq. (11) and get a compact relation valid in high dimensions:

$$\chi_{Bubble} = -2\int d\epsilon\, \mathcal{D}(\epsilon)\, \frac{d}{d\epsilon} n(\epsilon). \tag{12}$$

Here $\mathcal{D}(\epsilon) = \frac{2}{\pi D}\sqrt{1-\epsilon^2/D^2}$ is the band density of states per site per spin, and D is the half bandwidth.

For non-interacting electrons the function $n(\epsilon)$ is a constant with a unit jump at ϵ_F and we recover the standard result $\chi^0 = 2\mathcal{D}(\epsilon_F)$.

In the correlated problem, the jump at the Fermi energy is Z_k by Migdal's theorem, and so its contribution to χ_{Bubble} is Z_k. The background also contributes to the integral in Eq. (12), and it is important to understand its behavior as $n\to 1$. In Fig. (7) we display the momentum distribution at the three densities considered at two temperatures. We note that the entire variation of the monotonic function $n(\epsilon)$ is on the scale of δ; it settles down to a flat function $n(\epsilon) = 0.5$ *at* $n = 1^-$ and for small departures from half filling, the occupied (unoccupied) region is enhanced (depleted) by an area that is proportional to $\delta = 1-n$. Thus we see that as $n\to 1$, the background contribution is at most as large as δ, and thus χ_{Bubble} is a suitably weighted average of δ and Z. In the density regimes we are considering, the δ variation of Z is close to $\delta^{1.39}$ rather than δ (see discussion in Ref. (3)), and hence this balance can only be determined by a numerical evaluation. From Eq. (12) we can evaluate χ_{Bubble} and the results are shown from both theories at the three densities $\delta = .25, .2, .15$ in Fig. (8). Within ECFL it appears that χ_{Bubble} is dominated by the Migdal jump contribution; the spacing between the three relatively constant lines increases at lower δ. Within DMFT the situation appears to be reversed and χ_{Bubble} seems to scale with δ. In Fig. (6) we see that the DMFT results for Z/κ have a distinct positive slope relative to the ECFL results, and this is consistent with the above discussed differences in the computed χ_{Bubble} as well.

D. Self-energy and local density of states

In this section we study the imaginary part of the self energy $\rho_\Sigma(\omega) = -\frac{1}{\pi}\Im m\Sigma(\omega)$ and the (local) spectral function integrated over the band energies $\rho^{loc}_G(\omega) = -\frac{1}{\pi}\Im m\int d\epsilon\ \mathcal{D}(\epsilon)\, G(\epsilon,\omega)$. The results of the two theories,

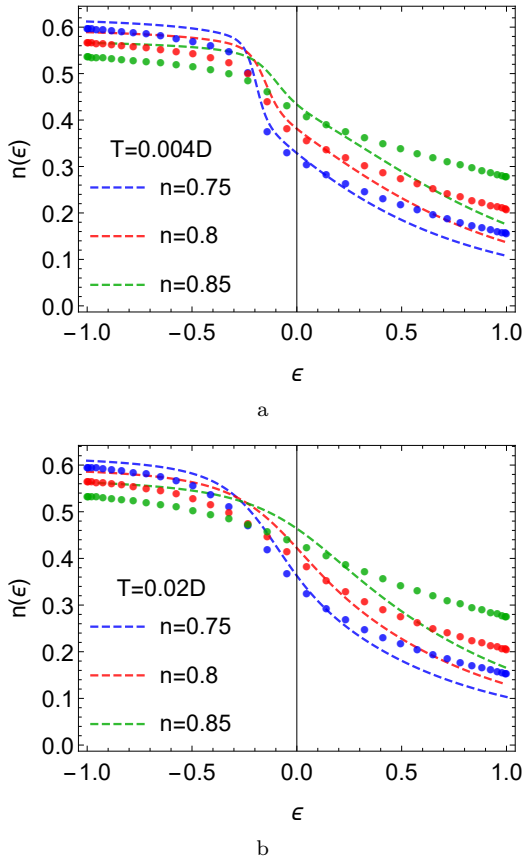

FIG. 7. The momentum distribution curves at three densities $n = .75, .8, .85$ (top to bottom at $\epsilon = -1$) at T=.004 D (panel (a)) and T=.02 D (panel (b)). The ECFL curves are solid symbols and the DMFT curves are dashed lines.

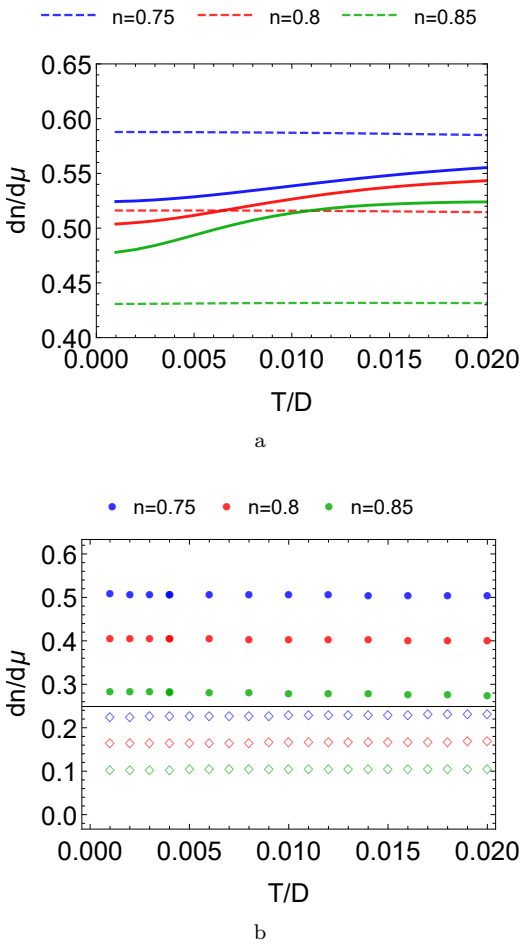

FIG. 8. The charge susceptibilities $\chi_c = dn/d\mu$, which are related to compressibility κ as $\chi_c = n^2\kappa$. The numerically exact values versus bubble estimates (Eq. (12)) in DMFT (full and dashed lines) and in panel (b) from ECFL (empty diamonds and solid circles).

including the magnitudes and their variation, are very close at low energies. The ECFL self-energy misses a maximum in $\rho_\Sigma(\omega)$ found in DMFT between $\omega \sim -0.1D$ and $\omega \sim -0.2D$. This feature was already noted in Ref. (3) and it is expected to influence the results of various quantities, such as the optical conductivity and dynamical Hall constant, but only at a fairly large energy. The imaginary part of the self energy in both theories shows a significant ω^3 type (i.e. odd in frequency) correction to the simple-minded expectation of a ω^2 behavior from Fermi liquid theory. This type of a skew has been argued in Ref. (41) to be responsible for the unusual and distinctive spectral functions in real materials- such as the cuprates.

The local spectral function of the two theories, shown in Fig. 10, are similar. They exhibit a sharpening of the maximum as n increases. Let us note that this object is relevant for angle integrated photoemission studies as well as STM studies, where one would also have to correct for the one electron density of states showing structure beyond that in the present theory.

E. Entropy and heat capacity

The heat capacity is computed in the ECFL theory by numerically differentiating the internal energy as $C_V = \partial E_K/\partial T$ on a fine T grid. From its numerical integration $\int_0^T dT' C_V(T')/T'$ we find the entropy. A similar procedure is used in the DMFT: the kinetic energies were computed on a equally spaced temperature grid (step size $\Delta T = 10^{-3}D$), numerically differentiated, smoothed using a Gaussian filter to obtain the heat capacity C_V, then interpolated using second-order polynomials, and finally integrated to obtain the entropy.

The heat capacity C_V is displayed in Fig. (11a). We note that C_V has a Schottky peak near $T \sim T_{FL}$ which becomes sharper as the density increases. At lower densities ($n = 0.7, 0.75$), a linear-T behavior is resolved, as we expect for a Fermi liquid. In Fig. (11b) we display C_V/T, from which we see that for densities closer to half-filling ($n = 0.8, 0.85$), the linear behavior of heat capacity is

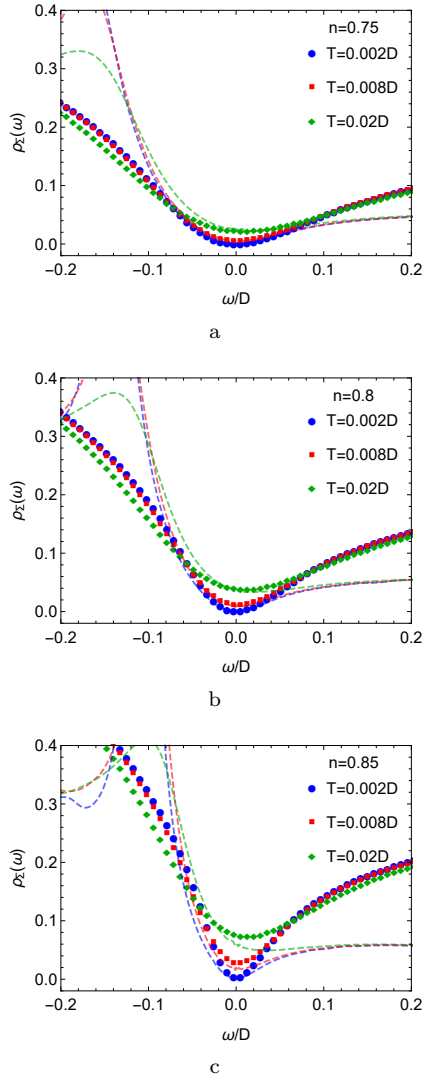

FIG. 9. Single particle decay rates, i.e. the spectral functions of self-energy ($\rho_\Sigma(\omega) = -\pi^{-1}\Im m\Sigma(\omega)$) of ECFL (symbols) and DMFT (dashed lines) for a range of temperatures.

not clearly resolved due to the small T_{FL} scale, and also due to increasing numerical uncertainties near half filling. Consequently, we find C_V/T appears to be growing as T decreases, instead of saturating. In Fig. (11c) we show the product of the heat-capacity slope $\gamma = C_V(T)/T$ and the quasiparticle residue Z at a low T corresponding to the GCFL regime. This product is expected to be a constant for localized Fermi liquids Ref. (24). At $\delta = 0.15$, we see however some variation in both ECFL and DMFT results. For higher hole densities $\delta = 0.2, 0.25$, it is indeed almost a constant.

In Fig. (12) we plot the entropy of the two theories, which give very similar results, and that of the free Fermi gas with a much lower entropy recovery at these temperatures. It is revealing to compare the heat capacity curve at $n = 0.8$ in Fig. (11a), with the resistivity results in Fig. (2) at the same densities. Both theories show a broad maximum in the heat capacity near the corresponding Fermi liquid temperature $T_{FL}(\delta)$, this is the temperature where the GCFL quadratic behavior of resistivity gives way to a linear behavior of the GCSM. At this temperature the entropy per site [See Fig. (12)] is $\sim 0.2\, k_B$, compared to the high T ($T = \infty$) value of 1.0119 k_B, obtained from $S_{ideal} \equiv S_{T=\infty} = k_B \{n \log 2 - n \log n - (1-n)\log(1-n)\}$. This corresponds to about 20% release of the entropy. For comparison, the Fermi gas on the Bethe lattice releases much less, about 1-2% entropy at a comparable T/D. At lower particle densities $n = 0.8, 0.75$ we again see that a $\sim 15-20\%$ release of the entropy occurs at the corresponding Fermi liquid temperature $T_{FL}(\delta)$, however the heat capacity has a more rounded behavior.

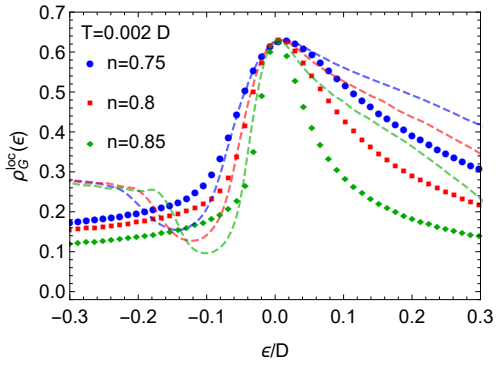

FIG. 10. Local density of states $\rho_G^{local}(\epsilon)$ of ECFL (symbols) and DMFT (dashed lines) at $T = 0.002D$.

In order to explore this further, in Fig. (13) we display the resistivity and the entropy recovery on the same T scale. We may thus take as a rule of thumb that at T_{FL}, the GCFL entropy release is $\sim 15 - 20\%$ relative to the maximum. This implies a substantial loss of coherence relative to the Fermi gas, i.e. the disordering of either the configurational (i.e. charge) degrees of freedom or to the spins. Below we study the magnetic susceptibility, to explore which of these is responsible. We find that the spins are largely unaffected when we go through T_{FL}, thereby implicating the charge degrees of freedom.

F. Magnetic Susceptibility

The uniform magnetic susceptibility close to the Mott transition, $n \gtrsim 0.75$, is one of the more difficult variables to compute reliably by any technique, since it is highly enhanced by Stoner factors $\chi_{spin}/\chi^0_{spin} \sim 10$. In the ECFL theory we found the numerical precision required for computing the susceptibility hard to achieve with the scheme outlined in Ref. (7). Although the local spectral functions for either spin are confined to a compact region in frequency, it is their difference that is needed for the susceptibility. This difference is numerically very small and smeared over a large frequency range

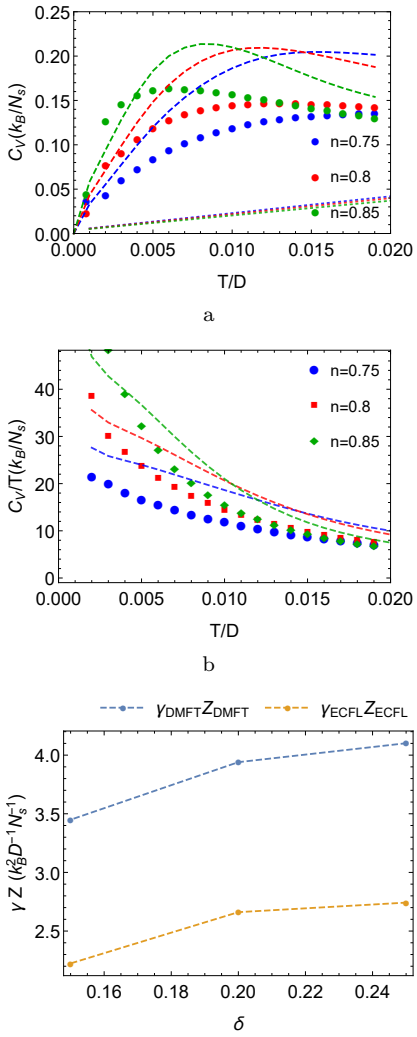

FIG. 11. (a) Specific heat computed from the kinetic energy by differentiation as $C_V = \partial E_K/\partial T$ for ECFL (symbols), DMFT (dashed lines) and free fermions (dotted lines). For $n = 0.8$ and $n = 0.85$ the heat capacity shows a gentle maximum at a characteristic T. (b) The ratio C_V/T versus T of ECFL (symbols) and DMFT (dashed lines). Taking the ratio with T wipes out the maximum seen in (a). (c) $\gamma \times Z$ at $T = 0.001D$.

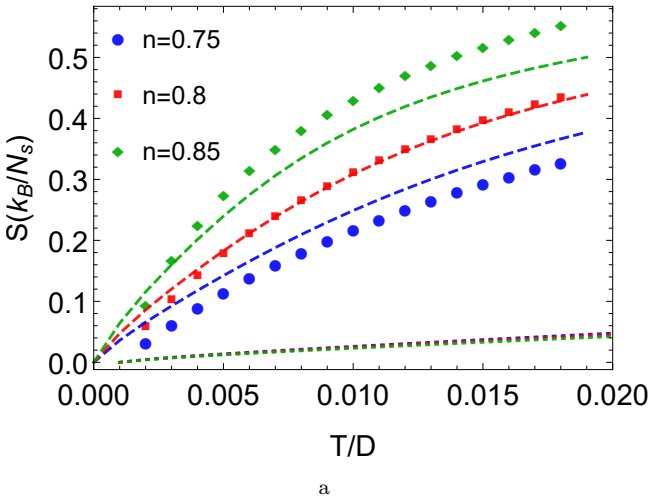

FIG. 12. The entropy versus T computed as $\int_0^T dT' C_V(T')/T'$ for ECFL (symbols), DMFT (dashed lines) and free fermions (dotted lines).

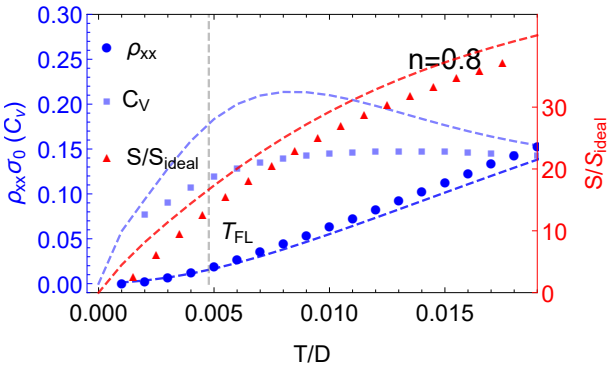

FIG. 13. Resistivity (blue circle), specific heat (light blue square) and entropy (red triangle) as percentage of the ideal entropy at infinite temperature S_{ideal}. The (Schottky) peak in the heat capacity is close to T_{FL}, the onset point of the linear-T resistivity or the end of the crossover region.

making it very difficult to control. The magnetic susceptibility χ is a sensitive variable also within the DMFT using the NRG as the impurity solver, in particular away from half filling at low temperatures, thus it is seldom studied using this approach (see, however Ref. (11 and 26) for some very early DMFT results, and Ref. (27) for a more recent study DMFT(NRG) of the half-filled Hubbard model in magnetic field at $T = 0$). With some effort we have found it possible to estimate its temperature dependence. We used the method of finite field[42,43] with $H = 10^{-4}D \ll T$, which is small enough for the system to remain well inside the linear response regime, but sufficiently large to be little affected by numerical noise. As a further test, we redid some calculations for $H = 10^{-3}D$, finding good consistency of the results.

In Fig. (14) we present the DMFT Stoner enhancement of the susceptibility $\chi_{spin}/\chi^0_{spin}$ as a function of T. Here the spin susceptibility is denoted by χ_{spin} and for non-interacting band case it is given by $\chi^0_{spin} = 2\mu_B^2\mathcal{D}(\varepsilon_F)$, where $\mathcal{D}$ is the band density of states per spin per site defined earlier. The scale of the Stoner enhancement is rather large, ~ 10. We find that the $T \to 0$ value is roughly consistent with $1/Z$, as expected for an almost localized Fermi liquid[24].

It is interesting that the Stoner factor and hence χ_{spin} is Pauli-like in the temperature range studied here, i.e. the GCFL and the GCSM regimes. It does not reflect the change in the resistivity behavior from quadratic to linear. Thus the magnetic contribution to the entropy change in Fig. (11) is very small, and we must infer that the GCSM regime continues to have a quenched spin en-

tropy, as in the Fermi liquid. It would appear, by inference, that the entropy released at T_{FL} is charge related and the crossover from the Fermi liquid to the GCSM may be viewed as partial charge disordering. This is to be contrasted to the cross-over from GCSM to the higher temperature bad metal regime, where the spin degrees of freedom do become partially unscreened[44,45].

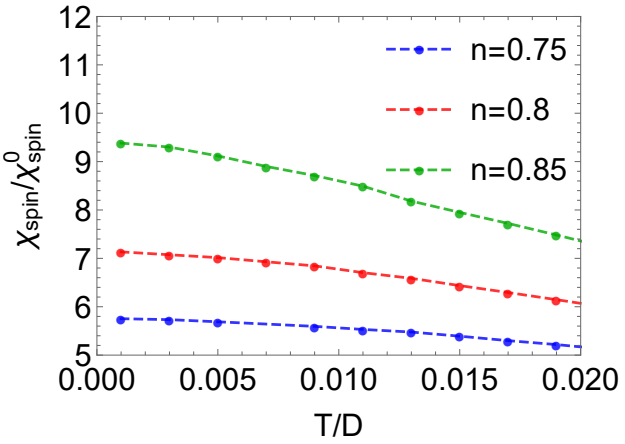

FIG. 14. Magnetic susceptibility (DMFT results). We note that the Stoner enhancement grows as $\delta \to 0$ and its T dependence is Pauli like, but with a somewhat enhanced T dependence at higher n. The crossover to linear resistivity occurs (see Fig. (2)) at fairly low $T \lesssim .005D$ at these densities, but has no reflection on the variation of χ_{spin}. We may thus infer that spin disordering is not relevant to the linear resistivity seen here.

G. Thermoelectric transport

For completeness we present the results for the thermopower S_t, the electronic thermal conductivity κ_e, and the Lorenz number L, as well as the thermoelectric figure of merit. We record the expressions following from standard transport theory Ref. (46), the thermopower S_t and electronic thermal conductivity κ_e are expressed in terms of three Onsager transport coefficients L_{11}, $L_{12} = L_{21}$ and L_{22} as follows:

$$\sigma_{xx} = e^2 L_{11}, \tag{13}$$

$$S_t = -\frac{k_B}{|e|T}\frac{L_{12}}{L_{11}}, \tag{14}$$

$$\kappa_e = \frac{k_B^2}{T}\left(L_{22} - \frac{L_{12}^2}{L_{11}}\right). \tag{15}$$

In infinite dimensions, these can be found in a straightforward way from the spectral functions due to vanishing vertex corrections:

$$L_{ij} = \frac{\sigma_0}{e^2}\int d\omega(-f'(\omega))\omega^{i+j-2}\int d\epsilon\, \Phi_{xx}(\epsilon)A^2(\omega,\epsilon). \tag{16}$$

The Lorenz number is

$$L = \frac{e^2}{k_B^2}\frac{\kappa_e}{\sigma_{xx}T}, \tag{17}$$

and the electronic thermoelectric figure of merit

$$ZT = T\sigma_{xx}S_t^2/\kappa_e. \tag{18}$$

In usual Fermi liquid theory, the electronic thermal conductivity $\kappa_e \sim T^{-1}$ and the thermopower $S_t \sim \gamma T$. The classic Lorenz number for a gas of particles with constant relaxation time is $L_0 = \pi^2/3$ when we set $k_B = |e| = 1$, while for Fermi liquid one expects $L_{\rm FL} = L_0/1.54 \approx 2.13$[47]. In previous DMFT studies[46,48–50], thermal transport coefficients were studied focusing on the very high temperature regime of the bad metals. While our results qualitatively agree with the previous studies, the crossover of thermal transport coefficients from GCFL to GCSM in the low-T regime (relative to the very high-T bad metal regime) are resolved for the first time. Both the thermopower and thermal resistivity of ECFL change slope near T_{FL}. In DMFT calculation, only the thermal resistivity shows similar crossover behavior, while the thermopower seems to be insensitive to the crossover from GCFL to GCSM. The Lorenz number of both ECFL and DMFT converges to $L \simeq 2.1$ in the low-T limit, as expected for a Fermi-liquid ground state. The low values of ZT, shown in Fig. 16(b), are typical of normal metals.

IV. CONCLUSIONS

This work achieves two goals. On one hand, we explored the low-temperature transport regimes of lattice fermions with the constraint of no double occupancy (Gutzwiller projection) in the limit of infinite dimensions. We focus on the temperature range where the Fermi-liquid quadratic resistivity gives way to the first T linear regime that we dubbed Gutzwiller correlated strange metal; this cross-over occurs on the temperature scale which is much lower compared with the bandwidth (and the Brinkman-Rice scale), but which actually corresponds to the experimentally most relevant range of order 100 K. On the other hand, this work had a further methodological goal of comparing the results for a number of transport, spectroscopic and thermodynamic quantities obtained using the mostly analytical extremely correlated Fermi liquid (ECFL) theory and the accurate numerical results from the dynamical mean field theory (DMFT) approach based on the numerical renormalization group as the impurity solver. We found that at the cross-over temperature scale both techniques indicate a change of behavior in most of the quantities we investigated. The two methods have generally good agreement, which improves upon lowering either the temperature or the density.

The origin of the cross-over in the resistivity has been tracked down to the temperature dependence of

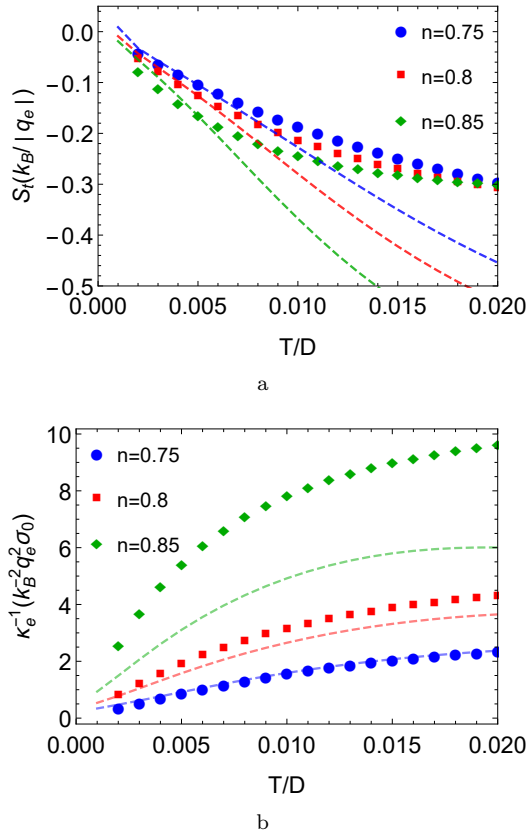

FIG. 15. (a) Thermopower of ECFL (symbols) and DMFT (dashed lines). Both amplitudes and temperature derivatives are similar for $T \leq .005$ but depart at higher T. (b) Electronic thermal resistivity κ_e^{-1} of ECFL (symbols) and DMFT (dashed lines).

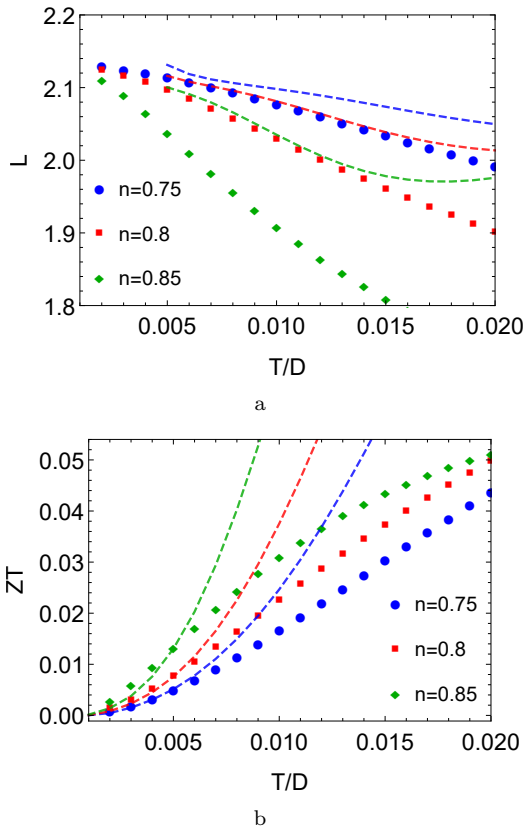

FIG. 16. (a) Lorenz number of ECFL (symbols) and DMFT (dashed lines). The Lorenz number saturates to a constant ($\simeq 2.1$) which is typically expected for a Fermi liquid at low temperatures. (b) Figure of merit for ECFL (symbols) and DMFT (dashed lines). The low values of ZT found here are typical of normal metals.

$-\Im m\Sigma(0,T)$, the imaginary part of the self-energy on the Fermi-surface, which starts to deviate from its low-temperature asymptotic behavior on the scale T_{FL} (Fermi-liquid temperature). This low-energy scale is produced by purely local Gutzwiller correlation effects, i.e., it is a direct consequence of the constraint of no double occupancy of the lattice sites. We managed to show that $\rho(T) \propto -\Im m\Sigma(0,T)$ (Eq. (7)), which accounts well for the $\rho(T)$ dependence in the (GCFL)-Fermi-liquid and (GCSM)-strange metal regimes. As a result, we are able to explain the temperature-dependence of the resistivity in terms of the temperature-dependence of the imaginary part of the self-energy on the Fermi-surface.

The charge compressibility of the DMFT theory at infinite U is seen to differ somewhat from that of the ECFL and also from the almost localized Fermi liquid. Developments in ECFL are underway in order to resolve the difference from DMFT. The compressibility shows a kink on the scale of T_{FL} and the heat capacity has a weak peak. The magnetic susceptibility, however, shows no change across this cross-over. The cross-over hence seems to be related to the charge degrees of freedom, while the spin entropy is quenched in both Fermi liquid and strange metal regimes. It thus seems that the GCSM regime has a highly unusual composition, with some disordering of the charges- presumably in anticipation of the incipient Mott insulating state, without the participation of the spins!

In a following paper Ref. (51), we present results for the dynamical Hall constant and Hall angle indicating that the two-relaxation-time behavior in transport properties observed in a number of cuprates emerges upon entering the GCSM regime. Finally we note a recent paper Ref. (52) where the results of a 2-dimensional version of the equations studied here are presented.

V. ACKNOWLEDGEMENTS

The work at UCSC was supported by the U.S. Department of Energy (DOE), Office of Science, Basic Energy Sciences (BES) under Award # DE-FG02-06ER46319. RŽ acknowledges the financial support from the Slovenian Research Agency (research core funding No. P1-0044 and project No. J1-7259). We thank Patrick Lee for

a stimulating discussion and Dieter Vollhardt for a helpful correspondence. This work used the Extreme Science and Engineering Discovery Environment (XSEDE[53] TG-DMR160144), which is supported by National Science Foundation grant number ACI-1053575, and the UCSC supercomputer Hyades, which is supported by National Science Foundation (award number AST-1229745) and UCSC.

[1] B. S. Shastry, Phys. Rev. Lett. **107**, 056403 (2011); *ibid* 108, 029702 (2012); Ann. Phys. (NY) **343**, 164 (2014).
[2] W. Metzner and D. Vollhardt, Phys. Rev. Lett. **62**, 324 (1989); A. Georges, G. Kotliar, W. Krauth, and M. J. Rozenberg, Rev. Mod. Phys. **68**, 13 (1996).
[3] R. Žitko, D. Hansen, E. Perepelitsky, J. Mravlje, A. Georges and B. S. Shastry, Phys. Rev. **B 88**, 235132 (2013), arXiv:1309.5284 (2013).
[4] A. Khurana, Phys. Rev. Letts. **64** , 1990 (1990)
[5] X.Y. Deng, J, Mravlje, R. Žitko, M. Ferrero, G. Kotliar and A. Georges, Phys. Rev. Lett. **110**, 086401 (2013).
[6] W. Xu, K. Haule, and G. Kotliar, Phys. Rev. Lett. **111**, 036401 (2013).
[7] B. S. Shastry and E. Perepelitsky, Phys. Rev. **B 94**, 045138 (2016), arXiv:1605.08213.
[8] Edward Perepelitsky, Andrew Galatas, Jernej Mravlje, Rok Žitko, Ehsan Khatami, B Sriram Shastry, and Antoine Georges, arXiv:1608.01600, Phys. Rev. **B 94**, 235115 (2016).
[9] E. Müller-Hartmann, Z. Phys. B: Condens. Matter, 74, 507 (1989)
[10] M. Jarrell, Phys. Rev. Lett., **69**, 168 (1992)
[11] M. Jarrell, Th. Pruschke, Phys. Rev. B, **49**, 1458 (1994)
[12] R. Zitzler, Th. Pruschke, R. Bulla, Eur. Phys. J. B, 27, 473 (2002)
[13] T. Pruschke, R. Zitzler, J. Phys.: Condens. Matter, 15, 7867 (2003)
[14] G. Sangiovanni, A. Toschi, E. Koch, K. Held, M. Capone, C. Castellani, O. Gunnarsson, S.-K. Mo, J. W. Allen, H.-D. Kim, A. Sekiyama, A. Yamasaki, S. Suga, P. Metcalf, Phys. Rev. B **73**, 205121 (2006)
[15] Robert Peters, Thomas Pruschke, Phys. Rev. B, **76**, 245101 (2007)
[16] Marcus Fleck, Alexander I. Liechtenstein, Andrzej M. Oleś, Lars Hedin, Vladimir I. Anisimov, Phys. Rev. Lett., **80**, 2393 (1998)
[17] R. Strack, D. Vollhardt, Phys. Rev. B, **46**, 13852 (1992)
[18] Yoichi Ando, Seiki Komiya, Kouji Segawa, S. Ono, and Y. Kurita Phys. Rev. Lett. **93**, 267001(2004).
[19] In the Gutzwiller approximation[20,21], double occupancy is projected out of the the Gutzwiller wave-function, while spin correlations are accounted for by purely combinatorial means. In Refs.[22,23], this approximation is derived diagrammatically, and shown to be exact in the limit of infinite spatial dimensions. In lower spatial dimensions, spin-correlations play a greater role, and hence the full Gutzwiller wave-function, with finite double-occupancy, must be used.
[20] M. C. Gutzwiller, Phys. Rev. **A 134**, 923 (1964).
[21] M. C. Gutzwiller, Phys. Rev. **A 137**, 1726 (1965).
[22] W. Metzner and D. Vollhardt, Phys. Rev. Lett. **59**, 121 (1987).
[23] W. Metzner and D. Vollhardt, Phys. Rev. **B 37**, 7382 (1988).
[24] D. Vollhardt, Rev. Mod. Phys. **56**, 99 (1984).
[25] D. Vollhardt, P. Wolfle and P.W. Anderson, Phys. Rev. **B 35** 6703 (1987).
[26] H. Kajueter, G. Kotliar, G. Moeller, Phys. Rev. B, **53**, 16214 (1996)
[27] J. Bauer, Eur. Phys. J. B **68**, 201 (2009).
[28] We are currently developing a few promising methods for yielding a closer quantitative agreement between the ECFL and DMFT for both quasiparticle residue Z and the resistivity at *all* densities.
[29] K. G. Wilson, Rev. Mod. Phys. **47**, 773 (1975)
[30] R. Bulla, T. Costi, Th. Pruschke, Rev. Mod. Phys. **80**, 395 (2008)
[31] R. Žitko, Th. Pruschke, Phys. Rev. B **79**, 085106 (2009)
[32] R. Žitko, Comp. Phys. Comm. 180, 1271 (2009)
[33] A. Weichselbaum, J. von Delft, Phys. Rev. Lett. **99**, 076402 (2007)
[34] R. Žitko, Phys. Rev. B **80**, 125125 (2009)
[35] R. Bulla, A. C. Hewson, Th. Pruschke, J. Phys.: Condens. Matter 10, 8365 (1998)
[36] The Ioffe-Regel-Mott resistivity is theoretically the largest value of resistance in an impure metal, attained when the mean free path is comparable to the lattice constant. Experimentally it has become standard to identify it with the largest resistivity attained in metallic systems exhibiting the phenomenon of resistivity saturation. This is seen in some strongly electron phonon coupled systems, such as the A-15 materials (e.g. Mo_3Ge, Nb_3Sb, or Nb_3Sn), where the T linear rise of the phonon scattering resistance rolls over and saturates. The suggested magnitude is from M. Gurvitch, Phys. Rev. B **24**, 7404 (1981), and Z. Fisk and G.W. Webb, Phys. Rev. Letts. **36**, 1084 (1976), corrected roughly for correlations.
[37] S. Martin, A. T. Fiory, R. M. Fleming, L. F. Schneemeyer and J. V. Waszczak, Phys. Rev. Lett. **60**, 2194 (1988).
[38] G. Bevilacqua, arXiv:1303.6206 (2013).
[39] The chemical potentials at the lowest T for the three densities in Fig. (5) are $0.72742, 0.98132, 1.35263$ for ECFL and $0.43986, 0.53668, 0.63789$ for DMFT.
[40] B. S. Shastry, E. Perepelitsky and A. C. Hewson, arXiv:1307.3492, Phys. Rev. **B 88**, 205108 (2013). DOI:http://dx.doi.org/10.1103/PhysRevB.88.205108
[41] B. S. Shastry, arXiv:1110.1032 (2011), Phys. Rev. Letts. **109**, 067004 (2012), G.-H. Gweon, B. S. Shastry and G. D. Gu, arXiv:1104.2631 (2011), Phys. Rev. Letts. **107**, 056404 (2011).
[42] M. J. Rozenberg, G. Kotliar and X. Y. Zhang, Phys. Rev. B **49**, 10181 (1994).
[43] A. Georges, G. Kotliar, W. Krauth and M. J. Rozenberg, Rev. Mod. Phys. **68**, 13 (1996).
[44] N. Dasari, N. S. Vidhyadhiraja, M. Jarrell, R. H. McKenzie, arXiv:1611.01822, (2016)
[45] J. Kokalj, Ross H. McKenzie, Phys. Rev. Lett., 110, 206402 (2013)
[46] B. S. Shastry, Rep. Prog. Phys. **72**, 016501 (2009), L.-F. Arsenault, B. S. Shastry, P. Semon, A.-M. S. Tremblay,

arXiv:1209.4349 (2012); Phys. Rev. B **87**, 035126 (2013)

[47] C. Herring, Phys. Rev. Lett. 19, 167 (1967); C. Herring, Phys. Rev. Lett. **19**, 684 (1967); L. V. Pourovskii, J. Mravlje, A. Georges, S. I. Simak, I. A. Abrikosov, arxiv:1603.02287 (2016).

[48] J. Merino and R. H. McKenzie, Phys. Rev. B **61**, 7996 (2000).

[49] V. Zlatić and J. K. Freericks, Phys. Rev. Lett. **109**, 266601 (2012).

[50] V. Zlatić, G. R. Boyd, and J. K. Freericks Phys. Rev. B **89**, 155101 (2014).

[51] *A Strange Metal from Gutzwiller correlations in infinite dimensions II: Transverse Transport, Optical Response and Rise of Two Relaxation Rates*, Wenxin Ding, Rok Žitko, and B. Sriram Shastry, arXiv:1705.01914

[52] *Extremely Correlated Fermi Liquid theory of the t-J model in 2 dimensions: Low energy properties*, B Sriram Shastry and Peizhi Mai, arXiv:1703.08142

[53] J. Town et al., "XSEDE: Accelerating Scientific Discovery", Computing in Science & Engineering, Vol.16, No. 5, pp. 62-74, Sept.-Oct. 2014, doi:10.1109/MCSE.2014.80